A GENEALOGY OF CONVEX SOLIDS VIA LOCAL AND GLOBAL BIFURCATIONS OF GRADIENT VECTOR FIELDS

GÁBOR DOMOKOS, PHILIP HOLMES AND ZSOLT LÁNGI

Abstract. Three-dimensional convex bodies can be classified in terms of the number and stability types of critical points on which they can balance at rest on a horizontal plane. For typical bodies these are nondegenerate maxima, minima, and saddle-points, the numbers of which provide a primary classification. Secondary and tertiary classifications use graphs to describe orbits connecting these critical points in the gradient vector field associated with each body. In previous work it was shown that these classifications are complete in that no class is empty. Here we construct 1- and 2-parameter families of convex bodies connecting members of adjacent primary and secondary classes and show that transitions between them can be realized by codimension 1 saddle-node and saddle-saddle (heteroclinic) bifurcations in the gradient vector fields. Our results indicate that all combinatorially possible transitions can be realized in physical shape evolution processes, e.g. by abrasion of sedimentary particles.

Contents

1991 *Mathematics Subject Classification.* 52A15 and 53A05 and 53Z05.
Key words and phrases. Codimension 2 bifurcation, convex body, equilibrium, Morse-Smale complex, pebble shape, saddle-node bifurcation, saddle-saddle connection.

1. Introduction

1.1. **Motivation and background.** The evolution of shapes of abrading bodies, such as pebbles in river beds and on beaches, has been studied for over 70 years (e.g. [23, 24, 25, 12, 3]). Data from NASA's Curiosity Rover on Mars [29, 18] has rekindled interest in the subject. In addition to classical shape indices such as axis ratios and roundness [27, 17], a recent approach considers the evolution of the number of *static equilibrium points* $N(t)$ on the surface of an abrading body, i.e., points on which the body can balance at rest on a horizontal plane [28, 9, 6, 5]. Unlike shape indices, which require length measurements, the integer $N(t)$ can be counted in simple experiments [9].

Abrasion occurs primarily on a body's convex hull, so to formulate a precise and relatively simple model we restrict our analysis to convex bodies K of uniform density, with surfaces described by scalar Euclidean distance functions r_K measured from the center of mass C_K. For such bodies static equilibria are critical points of r_K at which the gradient $\nabla r_K = 0$.

The surface ∂K of a generic convex body K can exhibit three types of nondegenerate critical points: local minima, maxima and saddle-points, which are sinks, sources and saddles of the gradient vector field $\mathbf{v} = \nabla r_K$. Let S, U, H respectively denote the number of each of these points. Since ∂K is a topological 2-sphere, the Poincaré-Hopf Theorem [2] implies that

$$S + U - H = 2. \tag{1}$$

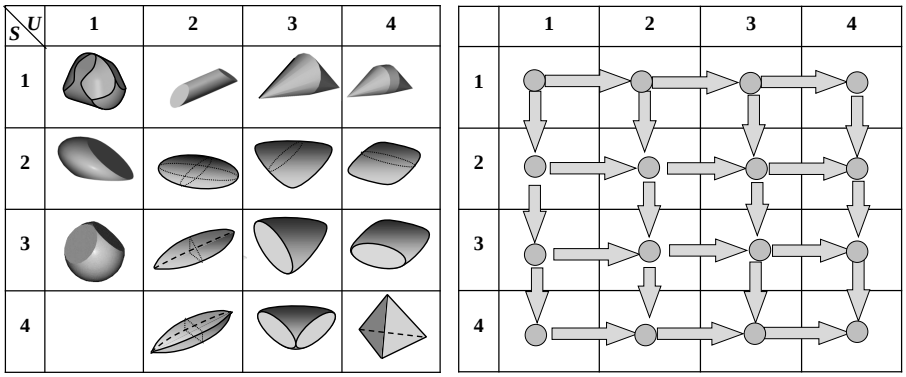

Figure 1. Primary equilibrium classes. Left: examples of convex bodies; rows and columns correspond to the numbers S and U of sinks and sources, respectively. Right: the 'Columbus Algorithm' of [28] defines a hierarchy among primary classes. Arrows indicate arbitrarily small truncations of the convex body, creating one additional sink or source and a saddle-point.

The classification schemes introduced in [28] are based on these numbers. Specifically, the *primary class* of a generic convex body K is defined as the pair of integers

$\{S, U\}$. In [28] it was shown that no primary class $\{i, j\}$ is empty and a hierarchy among these classes was defined via the *Columbus algorithm*. Using explicit truncations that remove small portions from K by slicing along convex surfaces, this algorithm generates a pair of convex bodies $K' \in \{i+1, j\}$ and $K'' \in \{i, j+1\}$, as shown in Figure 1. Thus, starting from the gömböc $\{1, 1\}$, every row and column can be populated, implying that the primary classification is complete in this 'static' sense.

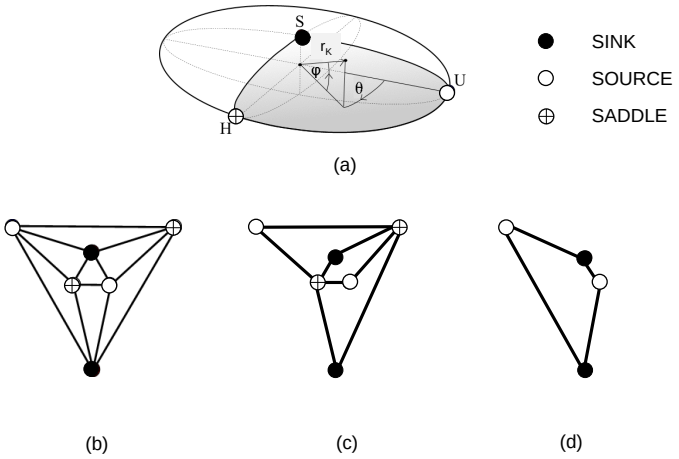

FIGURE 2. Graph representations of the gradient flow on the tri-axial ellipsoid in primary equilibrium class $\{2, 2\}$. (a) Distance function r_K given in spherical polar coordinates. (b) 3-colored quadrangulated primary representation $Q^3(\mathbf{v})$. (c) 3-colored triangulated representation $T^3(\mathbf{v})$. (d) Quasi-dual, 2-colored quadrangulated representation $Q^2(\mathbf{v})$. The colors refer to vertices, identifying them as sinks, sources, and (in (b,c)) saddles.

More refined methods exist for classifying the properties of gradient vector fields $\mathbf{v} = \nabla r_K$, including graph representations of their Morse-Smale complexes [10]. The vertices of these graphs are fixed points of $\mathbf{v}$, and the edges can be either isolated heteroclinic orbits connecting saddle-points, representative non-isolated heteroclinic orbits connecting saddles with sinks and sources, or both. These are called, respectively, the primary representation $Q^3(\mathbf{v})$, the triangulated representation $T^3(\mathbf{v})$, and the quasi-dual representation $Q^2(\mathbf{v})$ Figure 2 illustrates these representations for the tri-axial ellipsoid. For brevity, we call all three types the *topology graphs* associated with $\mathbf{v}$. Note that all three graphs $Q^3(\mathbf{v}), T^3(\mathbf{v})$, and $Q^2(\mathbf{v})$ are embedded on $\mathbb{S}^2$ and we will also consider their abstract, non-embedded versions $\bar{Q}^3(\mathbf{v}), \bar{T}^3(\mathbf{v})$ and $\bar{Q}^2(\mathbf{v})$. We remark that an abstract graph may have several, non-homeomorphic embeddings in $\mathbb{S}^2$. Precise definitions will be given in Section 2, and these graphs will play a key role in the paper.

We call the class of convex bodies with isomorphic abstract graphs the *secondary equilibrium class* and the class of convex bodies with homeomorphic embedded graphs the *tertiary equilibrium class* associated with K. See Figure 3(a), which

also illustrates that a primary class can contain different secondary classes: e.g., the ellipsoid is not alone in class $\{2, 2\}$. In [8] it was shown that the secondary and tertiary schemes are also complete in the sense that no secondary or tertiary class is empty.

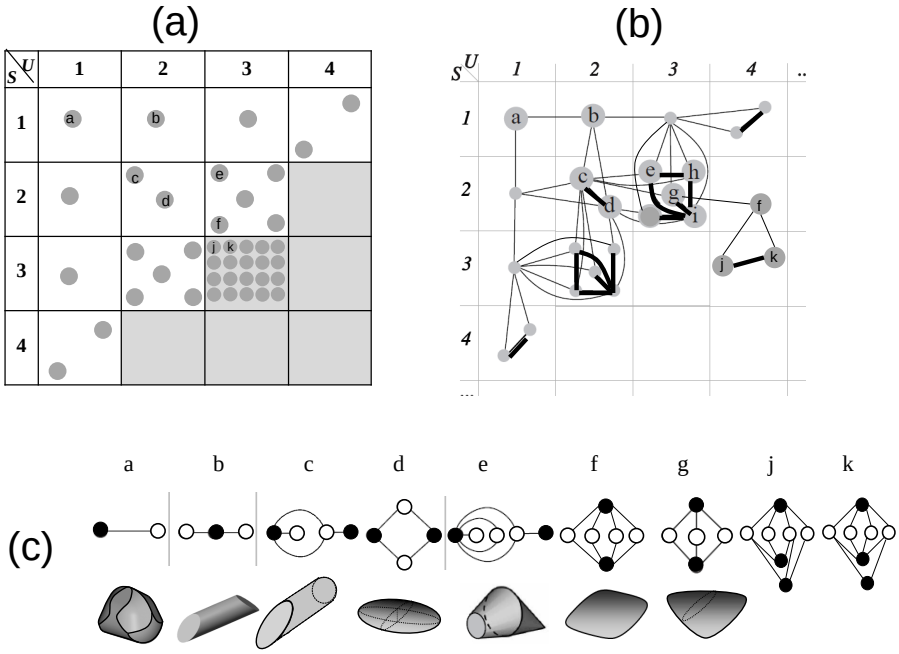

FIGURE 3. Secondary and tertiary equilibrium classes. (a) Secondary and tertiary classes are contained in primary classes. (b) Metagraph $\mathcal{G}$ with vertices at tertiary classes and edges corresponding to codimension 1 bifurcations; thin edges: saddle-nodes, thick edges: saddle-saddle bifurcations. Note that all illustrated secondary classes contain one tertiary class, so in the figure the vertices of the metagraph $\mathcal{G}$ correspond simultaneously to secondary and to tertiary classes. (c) Quasi-dual topology graphs $Q^2(\mathbf{v})$ of the tertiary classes labeled a through k in panels (a,b) and illustrations of a through g as convex bodies

One can ask whether transitions between different primary, secondary and tertiary classes are possible within generic families $K(\lambda)$ of smooth convex bodies, parametrized by λ, as their shapes change. In generic one-parameter families of gradient vector fields only two codimension 1 bifurcations occur: saddle nodes and saddle-saddle connections, and they do so at isolated, critical values $\lambda = \lambda_i^{cr}$ [14]. Saddle-nodes involve local changes in topology in which pairs of non-degenerate equilibria, either a saddle and a sink or a saddle and a source, emerge or disappear. Saddle-saddle bifurcations are global bifurcations at which an orbit connecting two saddle-points exists, but the numbers and types of equilibria do not change. In the

former, one of the integers S, U characterizing the primary class of K increases or decreases by one; in the latter, the primary class remains unchanged.

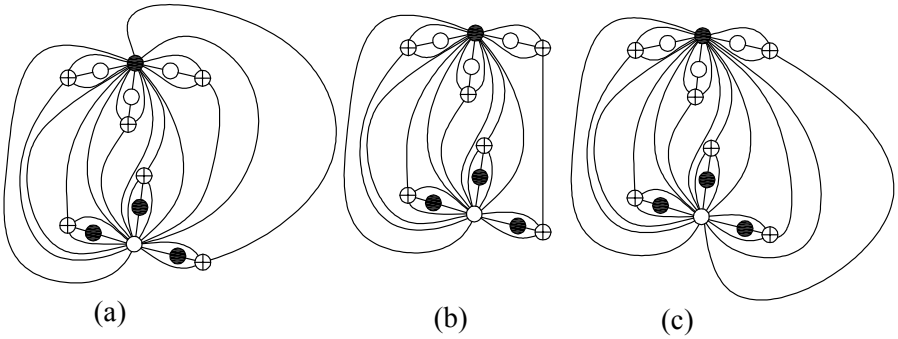

FIGURE 4. Topology graphs (a) and (c) corresponding to two vertices of $\mathcal{G}$ in primary equilibrium class $\{4, 4\}$ and the tertiary edge (b) connecting them. Graphs are shown in the triangulated representation of graph class $\mathcal{T}^3$. Note the saddle-saddle connection on (b), and that (a) and (c) are isomorphic as abstract graphs, but not homemorphic as embedded graphs on $\mathbb{S}^2$.

To visualize these transitions we introduce the metagraph $\mathcal{G}$ with vertices representing the embedded topology graphs associated with generic gradient fields on $\mathbb{S}^2$. The metagraph distinguishes *primary edges*, on which saddle-node bifurcations occur between vertices in different primary classes, from *secondary edges* that contain saddle-saddle bifurcations between vertices within the same primary class but in distinct secondary classes, and *tertiary edges* between vertices in the same secondary class. In Figure 3(b) primary and secondary edges are identified by thin and thick lines respectively. Figure 3 shows only primary classes with values $S+U \leq 6$; here tertiary edges cannot be illustrated since secondary classes with so few critical points contain only one tertiary class, and therefore have unique embeddings on the 2-sphere. Figure 4 illustrates a tertiary edge conecting two vertices in the primary class $\{4, 4\}$.

Our goal, which we will formally define in subsection 1.2, is to show that not only the vertices, but also the primary and secondary edges of $\mathcal{G}$ can be represented by convex bodies, i.e., physical processes describing their shape evolution may be represented by paths on $\mathcal{G}$. It is an intriguing question which of these paths are preferred by physical abrasion processes. The investigation of this question lies beyond the scope of the current paper, but we have some physical intuition on how primary classifications of convex bodies might evolve. In [5] it is shown that the evolution of S and U under the partial differential equations governing collisional abrasion processes can be modeled by letting S and U be random variables whose expected values decrease with time. While this trend has been verified both in laboratory experiments [6] and in the field [19], almost no pebbles in the primary classes $\{1, i\}, \{j, 1\}$, $(i, j = 1, 2, \dots)$ have been found. In [7] a purely geometrical reason for this phenomenon was pointed out. The difficulty of reducing either the number of sinks or sources can be measured by the fraction of volume that must

be removed from a solid, referred to as *robustness*. In [7] it was shown that the robustness of classes $\{2, i\}, \{j, 2\}$ is maximal so it is very unlikely that any natural pebble in these classes will be transformed into any of the classes $\{1, i\}, \{j, 1\}$ by natural abrasion.

Much less is known about the secondary, let alone tertiary classification of convex bodies, and theories for their evolution by abrasion are lacking. Nevertheless, as for the primary case, field data indicate that natural shapes strongly prefer some secondary classes while other classes remain virtually empty. Already in [15] it was observed that coastal pebbles tend to be ellipsoidal. While Rayleigh [23, 24, 25] Bloore [3] and Firey [12] ultimately showed that the classical *exact* ellipsoid is not an attracting state in collisional abrasion processes, nearly ellipsoidal shapes nonetheless dominate pebble beaches. Without exception, all those shapes in primary class $\{2, 2\}$ for which the secondary classes were determined have topology graph 'd' of Figure 3(c), while the other secondary class 'c' in $\{2, 2\}$ appears to be missing. Similar observations apply to other primary classes.

As a first step towards understanding these phenomena we show that the secondary classification scheme of [8] is also complete in the following 'dynamical' sense. Primary and secondary edges in the metagraph $\mathcal{G}$, containing codimension 1 saddle node and saddle-saddle bifurcations respectively, exist in the space of gradient vector fields $\mathbf{v} = \nabla r_K$ on the 2-sphere associated with convex bodies K. In the next subsection we use the metagraph $\mathcal{G}$ to formulate our statements and relate them to earlier results. Before doing so, we note that the gradient vector field $\mathbf{v} = \nabla r_K$ cannot describe the Newtonian dynamics of the body K rocking on a horizontal plane, which would require a system of second order differential equations, but that the stability types of its fixed points correctly reflect those of the equilibria of K.

1.2. **Definitions and main result.** We first define the metagraph $\mathcal{G}$, whose vertices are embedded topology graphs representing tertiary equilibrium classes associated with the Morse-Smale complexes [20] of gradient vector fields of convex bodies. For simplicity we use the primary representation $Q^3(\mathbf{v})$, but the triangulated or quasi-dual representations may also be used to construct $\mathcal{G}$. The edges of $\mathcal{G}$ correspond to codimension 1 bifurcations connecting these classes, and all possible one-parameter families of gradient vector fields on the 2-sphere appear in $\mathcal{G}$. We define the edges and vertices of $\mathcal{G}$ and we will use these concepts to formulate our results and relate them to earlier results.

Definition 1. Two vector fields $\mathbf{v}$ and $\mathbf{w}$ on the 2-sphere are *topologically equivalent* [26, 14] if their embedded topology graphs (of the same type) are homeomorphic.

As noted earlier, in case of generic vector fields [26], topology graphs can be defined by the Morse-Smale complex associated with the vector field [10]. Now we proceed to define the metagraph $\mathcal{G}$.

Definition 2. A vertex of $\mathcal{G}$ is an embedded topology graph $Q^3(\mathbf{v})$ on $\mathbb{S}^2$, associated with the Morse-Smale complex of a generic gradient vector field $\mathbf{v}$ on $\mathbb{S}^2$.

Definition 3. The primary class of a vertex $Q^3(\mathbf{v})$ is the pair of integers $\{S, U\}$, where S and U denote the number of sinks and saddles of $\mathbf{v}$. The secondary and

tertiary class of a vertex are the abstract graph $\bar{Q}^3(\mathbf{v})$ and the embedded graph $Q^3(\mathbf{v})$, respectively, both associated with the Morse-Smale complex of $\mathbf{v}$.

Definition 4. An edge of $\mathcal{G}$ is a one-parameter family $\mathbf{v}(\lambda), \lambda \in [0,1]$ of gradient vector fields connecting two distinct vertices $Q^3(\mathbf{v}(0))$ and $Q^3(\mathbf{v}(1))$ of $\mathcal{G}$. We require that $\mathbf{v}$ is generic except for a unique value $\lambda = \lambda^\star \in (0,1)$, for which $\mathbf{v}(\lambda^\star)$ exhibits a codimension 1 bifurcation [14].

Definition 5. We call an edge $\mathbf{v}(\lambda), \lambda \in [0,1]$ primary if the primary classes of $Q^3(\mathbf{v}(0))$ and $Q^3(\mathbf{v}(1))$ are different. We call an edge $\mathbf{v}(\lambda), \lambda \in [0,1]$ secondary if the primary class of $Q^3(\mathbf{v}(0))$ and $Q^3(\mathbf{v}(1))$ are identical, but their secondary classes are different. We call an edge $\mathbf{v}(\lambda), \lambda \in [0,1]$ tertiary if both the primary and the secondary class of $Q^3(\mathbf{v}(0))$ and $Q^3(\mathbf{v}(1))$ are identical.

Definition 6. We call a vertex $Q^3(\mathbf{v})$ of $\mathcal{G}$ physical if there exists a convex body K such that ∇r_K is topologically equivalent to $\mathbf{v}$.

Definition 7. We call a primary, secondary or tertiary equilibrium class physical if it contains at least one physical vertex.

Definition 8. We call an edge $\mathbf{v}(\lambda), \lambda \in [0,1]$ of $\mathcal{G}$ physical if there exists a one-parameter family $K(\lambda), \lambda \in [0,1]$ of convex bodies such that $\nabla r_K(\lambda)$ is topologically equivalent to $\mathbf{v}(\lambda)$ for all values of $\lambda \in [0,1]$.

Now we can formulate earlier and current results. Regarding primary equilibrium classes we have

Theorem 1. *All primary classes are physical.*

This result, proved in [28], was generalized in [8] to include secondary and tertiary classes:

Theorem 2. *All vertices of $\mathcal{G}$ are physical.*

In the current paper our goal is to further extend Theorems 1 and 2 by proving the physical existence of an important subset of edges of $\mathcal{G}$:

Theorem 3. *All primary and secondary edges of $\mathcal{G}$ are physical.*

1.3. **Sketch of proof.** As noted above, the local truncations constructed in [8] modify the Morse-Smale complex of K to produce one-parameter families of convex bodies in which either S or U is increased by 1. However, these families do not (necessarily) represent edges in the metagraph $\mathcal{G}$ since the genericity of the bifurcation was not guaranteed by the construction in [8]. One-parameter families connecting vertices at the ends of secondary edges (saddle-saddle bifurcations) were not even discussed in [8].

Here we extend these results by constructing a 2-parameter family of convex bodies whose gradient vector fields are generic in the sense that certain codimension 1 subsets (curves) in the parameter plane correspond to vector fields with codimension 1 local saddle-node and global saddle-saddle bifurcations, forming primary and secondary edges of $\mathcal{G}$. We also show that the codimension 1 bifurcation curves meet in a codimension 2 saddle to saddle-node bifurcation point.

Because secondary edges correspond to codimension 1 global saddle-saddle bifurcations, the local methods of [8] do not apply directly. Rather, we achieve our

goal in two steps. In Section 2 we prove Combinatorial Lemma 1, stating that any secondary edge of the metagraph $\mathcal{G}$ bounds a triangular face of $\mathcal{G}$ of which the two other edges are primary. As shown in Figure 9 below, the vertices of such a face represent three topology graphs that lie in adjacent primary classes of $\mathcal{G}$. The triangles (b,c,d) and (f,j,k) in Figure 3(b) above provide examples. We then appeal to dynamical systems theory [14] in Section 3 to show that such a triangular face could contain a codimension 2 bifurcation point for the gradient flow $\mathbf{v} = \nabla r_{K(\lambda)}$ and describe how codimension 1 saddle-node and saddle-saddle bifurcations emanate from this point.

In Section 4 we take the second step, providing an explicit geometrical construction that realizes the codimension 2 bifurcation via an arbitrarily small truncation of K depending on two parameters. First, in Subsection 4.1 we prove that a truncation exists under the assumption that the resulting displacement of the body's mass center has no effect on the topology of its gradient flow. Then, in Subsection 4.2 we construct a *simultaneous*, auxiliary truncation such that the mass center remains fixed under the combined truncations, implying that the topology of the flow is preserved. Finally, in Section 5 we summarize our results and point out some possible consequences.

2. Combinatorial part

Before stating the combinatorial lemma, we define three classes of graphs associated to Morse-Smale complexes on the 2-sphere, of which the graph representations introduced above and illustrated in Figure 2(b-d) are examples. As in [8], we denote by a *quadrangulation* a finite planar undirected multigraph on the 2-sphere in which each face is bounded by a closed walk of length 4 (cf. [1, 4]). A multigraph contains no loops but may have multiple (parallel) edges, and it is usually permitted that the boundary of a face may contain a vertex or an edge of the graph more than once (e.g. the faces with saddle-source and source-sink connections in Figure 5(a,c)). In addition, we follow Archdeacon et al. [1] and regard the *path graphs* (cf. [13]) P_2 and P_3 as quadrangulations, where P_k denotes a tree on k vertices, each with degree at most 2.

Dong et al. [10] introduced three different kinds of graph to represent a Morse-Smale complex on the 2-sphere, as follows:

- $\mathcal{Q}^2$ is the class of 2-vertex-colored quadrangulations. Note that as no quadrangulation contains odd cycles, each is 2-colorable (cf. [1, 21]). Furthermore, the coloring of the graph is unique up to switching the colors.
- $\mathcal{Q}^3$ is the class of 3-vertex-colored quadrangulations with $\deg(p) = 4$ for any $p \in H$, and $|\mathcal{S}| + |\mathcal{U}| - |\mathcal{H}| = 2$, where $\mathcal{S}$, $\mathcal{U}$ and $\mathcal{H}$ denote the sets of vertices of each given color.
- $\mathcal{T}^3$ is the class of 3-vertex-colored triangulations with $\deg(p) = 4$ for any $p \in \mathcal{H}$, and $|\mathcal{S}|+|\mathcal{U}|-|\mathcal{H}| = 2$, where $\mathcal{S}, \mathcal{U}$ and $\mathcal{H}$ denote the sets of vertices of each given color.

Examples of each class appear in Figure 5, panels (c,a,b) respectively.

It was shown in [11] (cf. [30]) that a Morse-Smale complex on the 2-sphere can be uniquely represented by a 3-vertex-colored quadrangulation in $\mathcal{Q}^3$, where the

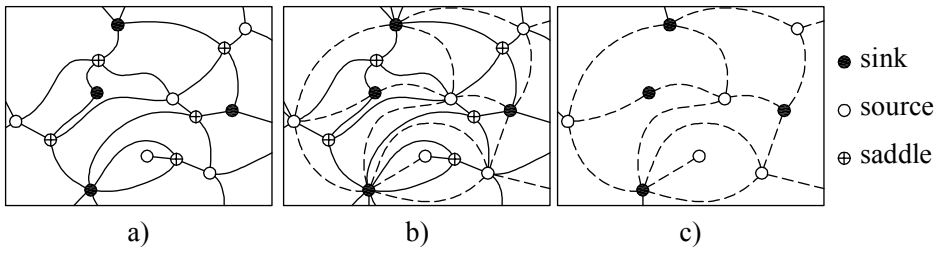

FIGURE 5. Different representations of a part of a Morse-Smale complex. (a) Primary topology graph in class $\mathcal{Q}^3$. (b) Triangulated topology graph in class $\mathcal{T}^3$. (c) Quasi-dual topology graph in class $\mathcal{Q}^2$.

vertex colors represent the 3 types of critical points (maxima, minima and saddles) and edges correspond to stable and unstable manifolds: isolated integral curves that end and start at saddle points. Each quadrangle is bounded by a closed walk consisting of a source, a saddle, a sink and a saddle in cyclic order around the face and, and every saddle has degree 4; see Figure 6(a). Following Dong et al. [10] we call this the *primary* topology graph.

Saddle points can be removed from the primary graph without losing information [10]: first we connect sources and sinks inside each quadrangle, producing a *triangulated* topology graph in class $\mathcal{T}^3$; we then remove all saddle points and edges incident to them, as in Figures 5(b,c). Since non-degenerate saddles have degree 4, the resulting graph is a 2-vertex-colored quadrangulation in class $\mathcal{Q}^2$: the *quasi-dual* topology graph (cf. [10]). Here we use the latter; however, in Section 4, the primary graph representation is preferable. All three representations are equivalent in the sense that they are mutually uniquely identified.

Let $F = (p_1, p_2, p_3, p_4)$ be a face of any $Q \in \mathcal{Q}^2$ (cf. Figure 6(a), left). Pairs of vertices, and/or edges connecting them, may coincide. Nonetheless, a quasi-dual representation admits only two kinds of coincidences: two diagonally opposite vertices, say p_2 and p_4 may coincide, and in this case two consecutive edges, say (p_4, p_1) and (p_1, p_2) may coincide: these two cases are illustrated in Figures 6(b) and (c), left. Note that in Figure 6(c) the internal domain bordered by the edges (p_4, p_1) and (p_1, p_2) is not a quadrangular face and necessarily contains at least one additional vertex, as indicated by the triangles in the inner region. Figure 6(d) shows the remaining two exceptional cases: the trees $Q = P_3$ and $Q = P_2$.

The algorithm in [8] is based on repeated application of a combinatorial graph operation called *face contraction* (cf. [1, 4] or [22]). Applied to the face F defined in the previous paragraph, this operation results in the contraction of the vertices p_1 and p_3 into the same vertex, and the disappearance of F; the modified graphs, depending on the 'shape' of the original face F are shown on the right of each panel in Figure 6. The inverse operation of face contractions is called *vertex splitting*. Combinatorially, for graphs with at least three vertices it can be defined as follows. Let p be a vertex of the quadrangulation Q, with adjacent edges $E_1, E_2, \ldots, E_k, E_{k+1} = E_1$ in counterclockwise order, and note that the

other endpoints of some of these edges may coincide. Choose two, not necessarily distinct edges: E_x and E_y. Then we split p into two vertices p_1 and p_3, and E_x and E_y into two pairs of edges $E_{x,1}$ and $E_{x,3}$, and $E_{y,1}$ and $E_{y,3}$, such that $E_{x,1}, E_{x+1}, \ldots, E_{y-1}, E_{y,1}$ are connected to p_1, and $E_{y,3}, E_{y+1}, \ldots, E_{x-1}$ and $E_{x,3}$ are connected to p_3. This operation can be naturally modified for primary and triangulated representations: in the primary representation, instead of two edges we choose two (not necessarily distinct) faces, whereas in a triangulated representation we choose two edges connecting a sink and a source.

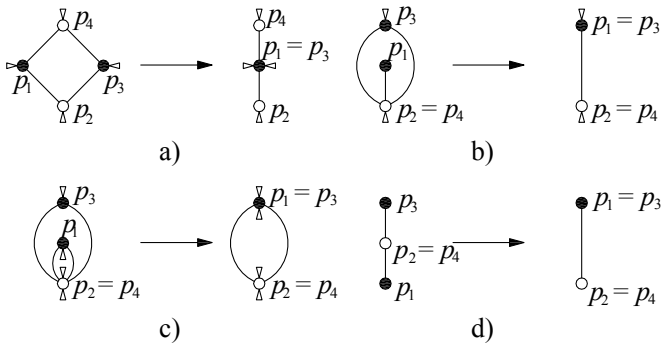

FIGURE 6. Face contractions on a graph in class $\mathcal{Q}^2$. As in [4], triangles incident to some vertices indicate that one or more edges *may* occur at that position around the vertex. Here p_1 and p_3 are sinks; analogous face contractions, each removing a source from the graph, can be performed by switching the colors.

In a quasi-dual graph, a transition via a saddle-saddle connection can be realized as a *diagonal slide* [22], defined as follows: consider two faces (v_1, v_2, v_3, v_4) and (v_4, v_3, v_5, v_6) of the quadrangulation sharing an edge (v_3, v_4), and replace this edge either by (v_1, v_5) or (v_2, v_6). Then the two faces (s_1, u_3, s_2, u_2) and (u_1, s_3, u_2, s_2) are replaced by (s_1, u_3, s_3, u_2) and (u_1, s_3, u_3, s_2).

To formulate the lemma, we need the following definition.

Definition 9. Let $Q \in \mathcal{Q}^2$ be a quadrangulation. Two vertex splittings W and W' of Q are called *twin*, if:

- The same vertex p is split.
- Let A_1 and A_2 denote the sets of edges connected to the two split vertices in W, and define A_1' and A_2' similarly for W'. Then A_1 differs in exactly one element from A_1' or A_2'.

In this case Q is called the *ancestor* of the two split graphs. This definition can also be naturally interpreted for primary and triangulated representations.

Note that the second property in Definition 9 implies that A_2 also differs in exactly one element from A_1' or A_2'. The graphs in columns B and C of rows (a) and (b) in Figure 7 can be obtained from the graph in column A of the same row via twin vertex splittings, but the graphs in columns B and C of Figure 7(c) are

isomorphic and hence have no ancestor graph. This corresponds to the degenerate case 3 in the Proof of the Combinatorial Lemma 1 below.

Lemma 1 (Combinatorial Lemma)**.** *Let $B, C \in \mathcal{Q}^2$ be embeddings of two distinct abstract graphs $\bar{B}, \bar{C}$ in $\mathbb{S}^2$, respectively, such that there is a diagonal slide that transforms B into C. Then there is an embedding $A \in \mathcal{Q}^2$ and a pair of* twin *vertex splittings W_B and W_C of $\bar{A}$ such that W_B transforms A into B, and W_C transforms A into C.*

We remark that, as we will see in the proof of Lemma 1, there are diagonal slides between non-homeomorphic drawings of the same graph which cannot be derived from the same ancestor via twin vertex splittings. Note also the essential condition that the abstract graphs $\bar{B}, \bar{C}$ should be non-isomorphic; this condition excludes tertiary edges from our argument.

Proof. To simplify the proof, we use the triangulated variants of B and C, which with a little abuse of notation, we also denote by B and C. Let the two saddles that are connected by the saddle-saddle bifurcation be denoted by h_1 and h_2. This edge belongs to two faces of B, say (s_2, u_1, h_1) and (s_2, u_1, h_2), and similarly, two faces of C, say (s_1, u_2, h_1) and (s_1, u_2, h_2). We note that, due to the degeneracy of the graph, some of the vertices or edges may coincide; nevertheless, due to the saddle-saddle connection, h_1 and h_2 are distinct.

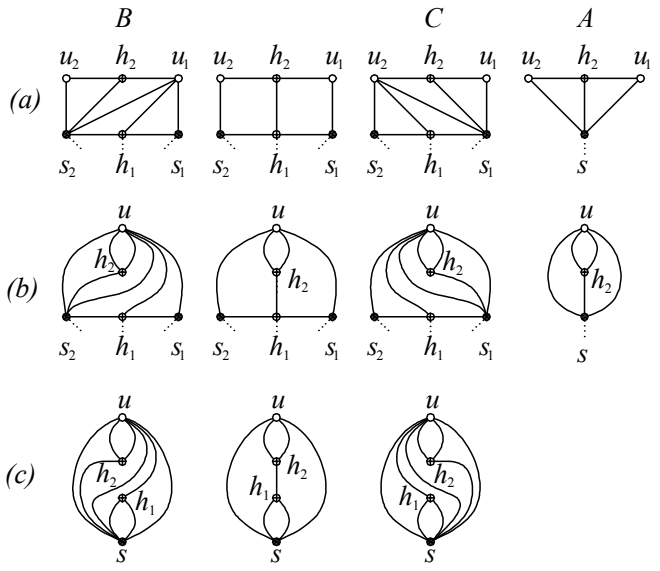

FIGURE 7. The connection between diagonal slides and twin vertex splittings for $\mathcal{T}^3$-class graphs. The graphs in row (c), columns B and C are isomorphic, and thus have no common ancestor, hence no graph appears in column A of row (c). See the proof of Lemma 1 for further details.

Case 1, s_1 and s_2, and also u_1 and u_2 are distinct. Figure 7 row (a) shows the corresponding faces of B, the saddle-saddle bifurcation, C, and the common

ancestor A from left to right. Face contractions are carried out by collapsing the edges (s_1, h_1) and (s_2, h_1) into a single vertex s, and the dotted edges starting at s_1, h_1 and s_2 are contracted into the single dotted edge of A. Furthermore, the edges (s_2, u_1), (h_1, u_1) and (s_1, u_1) are contracted to (s, u_1) in B, whereas (s_2, u_2), (h_1, u_2) and (s_1, u_2) are contracted to (s, u_2) in C. Since (s, u_1) and (s, u_2) are consecutive edges of A in the quasi-dual representation, the vertex splittings belonging to the two face contractions are indeed twin. We remark that in Case 1 another ancestor can be found by contracting (u_1, h_2) and (u_2, h_2).

Case 2, exactly one of the pairs $\{s_1, s_2\}$ or $\{u_1, u_2\}$ coincide. Without loss of generality, we may assume that $u_1 = u_2 = u$ and $s_1 \neq s_2$. Note that as the degree of a saddle point is 4, in this case there are two edges starting at h_2 and ending at u. Figure 7 row (b) shows the corresponding faces of B, the saddle-saddle bifurcation, C, and the common ancestor A from left to right. Face contraction is carried out by collapsing the edges (s_1, h_1) and (s_2, h_1) into a single vertex s.

Case 3, $s_1 = s_2 = s$, and $u_1 = u_2 = u$. In this case B and C are isomorphic graphs: Figure 7 row (c). We note that in this case the two edges starting at s and ending at u may also coincide.

□

3. Dynamical part

In this section we describe how codimension 1 saddle-node and saddle-saddle bifurcations can meet in a codimension 2 bifurcation of a gradient vector field $\mathbf{v}$ on $\mathbb{S}^2$. Such a bifurcation point can be associated with each triangular face of the metagraph $\mathcal{G}$ having two primary edges and one secondary edge. We construct an explicit polynomial function $V_{\mu_1,\mu_2}(x, y)$, depending on two parameters μ_1, μ_2, that captures the behavior of $\mathbf{v}$ near a degenerate saddle-node whose strong stable manifold contains one branch of the unstable manifold of a non-degenerate (hyperbolic) saddle point. The parameters μ_1, μ_2 provide local coordinates on the face of the metagraph near the codimension 2 point. Since the saddle-saddle or *heteroclinic* connection is a global phenomenon, our vector field will necessarily be non-local, but we can nonetheless find a cubic potential function that captures the local saddle-node and the global heteroclinic connection. A *homoclinic* orbit to a saddle-node bifurcation point was previously shown to occur in the averaged equations for the periodically forced van der Pol oscillator [16], cf. [14, Sec. 2.1,Figs. 2.1.2-3].

We first recall the normal form of an isolated codimension 1 saddle-node in a gradient vector field on the plane, which can be described by a potential function depending on one parameter [14]:

$$V_{\mu_1}(x, y) = \frac{x^3}{3} + \frac{y^2}{2} - \mu_1 x, \tag{2}$$

The corresponding vector field

$$\begin{aligned} \dot{x} &= -\tfrac{\partial V_{\mu_1}}{\partial x} = -x^2 + \mu_1, \\ \dot{y} &= -\tfrac{\partial V_{\mu_1}}{\partial y} = -y, \end{aligned} \tag{3}$$

has no fixed points for $\mu_1 < 0$, a saddle-node at $(x, y) = (0, 0)$ for $\mu_1 = 0$, and a hyperbolic saddle and a sink at $(x, y) = (-\sqrt{\mu_1}, 0)$ and $(+\sqrt{\mu_1}, 0)$ respectively for $\mu_1 > 0$.

We now add further cubic terms and a linear term containing another parameter μ_2 to V_{μ_1} to produce a second hyperbolic saddle that can be displaced relative to the saddle and sink described above. We set

$$V_{\mu_1,\mu_2,\alpha}(x,y) = \frac{x^3}{3} + \frac{y^2}{2} + \frac{y^3}{3} - \alpha x^2 y - \mu_1 x - \mu_2 xy, \text{ with } \alpha \geq (1/4)^{1/3}, \tag{4}$$

so that the vector field (3) becomes

$$\begin{aligned} \dot{x} &= -x^2 + 2\alpha xy + \mu_1 + \mu_2 y, \\ \dot{y} &= \alpha x^2 - y - y^2 + \mu_2 x. \end{aligned} \tag{5}$$

Elementary calculations and linearization at the fixed points show that, for $\mu_1 = \mu_2 = 0$, the saddle node remains at $(0,0)$ and a hyperbolic saddle lies at $(0,-1)$. Moreover, the y-axis is an invariant line, because $\dot{x} \equiv 0$ for any solution with initial condition $(0, y_0)$. The unstable manifold of the saddle $(0,-1)$ is the line segment $\{x = 0 | y \in (-\infty, 0)\}$, the upper part of which coincides with the the lower part of the strong stable manifold $\{x = 0 | y \in (-1, +\infty)\}$ of the saddle-node. A disk containing these two fixed points constitutes a chart, containing the codimension 2 degenerate vector field, that can be mapped onto a an open set of $\mathbb{S}^2$: see Figure 8(b). The term $-\alpha x^2 y$ is necessary to make the lower saddle hyperbolic (its eigenvalues are -2α and $+1$). A second hyperbolic saddle lies at $(2\alpha/(4\alpha^3 - 1), 1/(4\alpha^3 - 1))$, but this fixed point is irrelevant to the bifurcations of interest, and it can be driven out of any compact region by letting $\alpha \to (1/4)^{1/3} \stackrel{\text{def}}{=} \alpha^* \approx 0.62996$. For the cases shown in Figure 8(b-j) we set $\alpha = 0.62996$.

We now describe the codimension 1 bifurcations and structurally stable vector fields that emerge from the codimension 2 bifurcation point for small μ_1, μ_2. Setting $\dot{x} = \dot{y} = 0$ in (5), and noting that $y = (x^2 - \mu_1)/(2\alpha x + \mu_2)$ from the first equation, we may eliminate y from the second equation to obtain the fixed point condition

$$F_{\mu_1,\mu_2,\alpha}(x) = a_4 x^4 + a_3 x^3 + a_2 x^2 + a_1 x + a_0 = 0, \tag{6}$$

where

$$\begin{aligned} &a_4 = 4\alpha^3 - 1, \ a_3 = 2\alpha(4\alpha\mu_2 - 1), \ a_2 = 2\mu_1 + 5\alpha\mu_2^2 - \mu_2, \\ &a_1 = 2\alpha\mu_1 + \mu_2^3 \ \text{ and } \ a_0 = \mu_1\mu_2 - \mu_1^2. \end{aligned} \tag{7}$$

For $\mu_1 = \mu_2 = 0$ Eqn. (7) becomes $((4\alpha^3 - 1)x - 2\alpha)x^3 = 0$, with a triply-degenerate root at $x = 0$ and the irrelevant root at $x = 2\alpha/(4\alpha^3 - 1)$. Setting $\alpha = \alpha^*$ so that the latter root lies at ∞, the quartic polynomial becomes a cubic with discriminant

$$\Delta = 18 a_0 a_1 a_2 a_3 - 4 a_0 a_2^3 + a_1^2 a_2^2 - 4 a_1^3 a_3 - 27 a_0^2 a_3^2. \tag{8}$$

To obtain an explicit approximation for the saddle-node bifurcation curve $\mu_1 = f_1(\mu_2; \alpha^*)$, we consider this special case. Substituting the expressions (7) into (8) and setting $\Delta = 0$ yields a polynomial relating μ_1 and μ_2 for which $F_{\mu_1,\mu_2,\alpha^*}(x_0) = F'_{\mu_1,\mu_2,\alpha^*}(x_0) = 0$ and one of relevant roots x_0 is multiple. Except for $\mu_1 = \mu_2 = 0$, for which $x_0 = 0$ and $F''_{\mu_1,\mu_2,\alpha^*}(0) = 0$, this is a double root, and it corresponds either to a saddle-node bifurcation, or to the heteroclinic saddle-saddle connection discussed below. Expanding μ_1 in integer powers of μ_2 and using the fact that $a_3 = -2\alpha + \mathcal{O}(\mu_2)$ to determine the leading terms, we find the following expression for the saddle-node bifurcation:

$$\mu_1 = f_1(\mu_2; \alpha^*) = -\frac{\mu_2^4}{4} - \frac{3 \cdot 2^{1/3} \mu_2^5}{8} - \frac{5 \cdot 2^{2/3} \mu_2^6}{8} + \mathcal{O}(\mu_2^7). \tag{9}$$

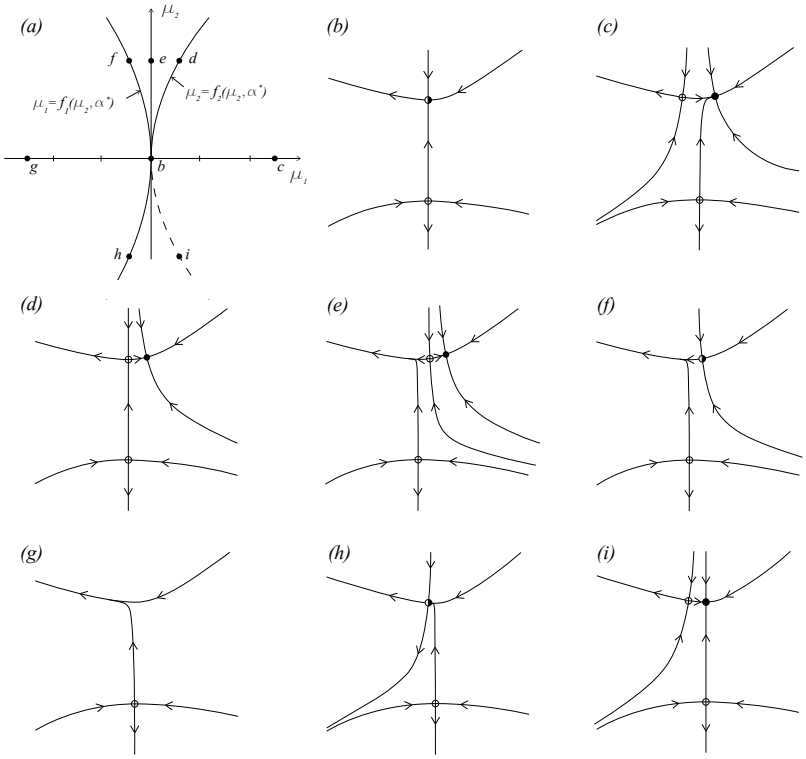

FIGURE 8. Bifurcations of the gradient vector field (5). (a) The bifurcation set in (μ_1, μ_2)-space near the codimension 2 point $(0, 0)$: saddle-nodes occur on the curve $\mu_1 = f_1(\mu_2; \alpha) \neq 0$; saddle-saddle connections exist on the curve $\mu_1 = f_2(\mu_2; \alpha) = \{\mu_2^2/4\alpha^2 | \mu_2 \in (0, \sqrt{\alpha})\}$. (b) At $\mu_1 = \mu_2 = 0$ the unstable manifold of the saddle at $(0, -1)$ lies in the strong stable manifold of the saddle-node at $(0, 0)$. (c) For $\mu_1 > \max\{f_1(\mu_2; \alpha), f_2(\mu_2; \alpha)\}$ two unconnected hyperbolic saddles coexist with a sink. (d) Along $\mu_1 = f_2(\mu_2; \alpha) < \alpha^2$ with $\mu_2 > 0$ a codimension 1 saddle-saddle connection exists on the invariant line $x = -\sqrt{\mu_1}$. (e) For $f_1(\mu_2; \alpha) < \mu_1 < f_2(\mu_2; \alpha)$ and $\mu_2 > 0$ two hyperbolic saddles and a sink exist with the lower saddle's unstable manifold passing left of the upper saddle's stable manifold. (f) On $\mu_1 = f_1(\mu_2; \alpha) < 0$ with $\mu_2 > 0$ a codimension 1 saddle-node occurs with the lower saddle's unstable passing to its left. (g) For $\mu_1 < f_1(\mu_2; \alpha)$ only the lower saddle exists. (h) On $\mu_1 = f_1(\mu_2; \alpha) < 0$ with $\mu_2 < 0$ a codimension 1 saddle-node occurs with the lower saddle's unstable entering from its right. (i) Along $\mu_1 = f_2(\mu_2; \alpha)$ with $\mu_2 < 0$ the lower saddle's unstable manifold lies on the invariant line $x = -\sqrt{\mu_1}$ and intersects the strong stable manifold of the sink; this is *not a bifurcation point.*

As in Eqn. (3), μ_1 primarily controls the saddle-node bifurcation, but the second parameter μ_2 shifts the relative x positions of the upper and lower saddles, allowing a codimension 1 heteroclinic connection to form with $\mu_1 \neq 0$. Specifically, along the curve

$$\mu_1 = f_2(\mu_2;\alpha) = \frac{\mu_2^2}{4\alpha^2}, \quad \text{with} \quad \mu_2 \in (0,\sqrt{\alpha}), \tag{10}$$

both saddle points lie on the invariant line $x = -\sqrt{\mu_1}$ and a connecting orbit from the lower to the upper saddle exists (their y coordinates are $\frac{1}{2}\left[-1 \mp \sqrt{1-\mu_2^2/\alpha}\right]$ respectively). This bifurcation curve is shown in Fig. 8(a) for $\alpha = \alpha^*$, together with the saddle-node curve $\mu_1 = f_1(\mu_2;\alpha^*)$ (the latter's curvature is exaggerated for clarity). Note that the discriminant $\Delta = 0$ for $\mu_1 = \mu_2^2/4\alpha^{*2}$ since both saddles have the same x-coordinate. A similar invariant line $x = +\sqrt{\mu_1}$ connects the lower saddle to the strong stable manifold of the sink for $\mu_1 = \mu_2^2/4\alpha^2$ with $\mu_2 < 0$, but since saddle-sink connections are structurally stable, no bifurcation occurs here (Figure 8(j)).

In addition to the degenerate codimension 2 vector field at $(\mu_1,\mu_2) = (0,0)$ shown in panel (b), panels (c-h) show representative vector fields on the codimension 1 bifurcation curves and structurally-stable vector fields in the three open regions in the bifurcation set of panel (a). For the unfolding parameters used here, the saddle-node and saddle-saddle connection bifurcation curves meet in a quadratic tangency at $(\mu_1,\mu_2) = (0,0)$. The geometrical parameters (d,ϕ) chosen in the construction that follows produce bifurcation curves that meet transversely at $(0,0)$, as shown in Figure 9.

4. Geometrical part

In this section we prove Theorem 3. To do this, it suffices to create for any primary or secondary edge $E = \{v_1, v_2\}$ of the metagraph $\mathcal{G}$ a *suitable,* one-parameter family $K(\lambda)$ of convex bodies, where $\lambda \in [\lambda_1, \lambda_2]$, with a unique value $\lambda^\star \in (\lambda_1, \lambda_2)$ such that the graph of $K(\lambda)$ is homeomorphic to v_1 for any $\lambda \in [\lambda_1, \lambda^\star)$, homeomorphic to v_2 for any $\lambda \in (\lambda^\star, \lambda_2]$, and to the graph of the 1-codimension bifurcation defined by $E = \{v_1, v_2\}$ at $\lambda = \lambda^\star$. In this case we can choose a re-parametrization of this family that will satisfy the topological equivalence condition of the theorem.

We prove the assertion only for secondary edges of $\mathcal{G}$, because for primary edges we may apply a simpler version of the same argument. As noted before, our argument does not apply to tertiary edges. Secondary edges correspond to non-local bifurcations, so it is hard to construct by local truncations a suitable one-parameter family of convex bodies that corresponds to any given secondary edge. To ensure that local truncations suffice, we rely on Lemma 1, stating that any secondary edge belongs to a triangular face of $\mathcal{G}$ of which the two other edges are primary. Since the latter correspond to local saddle-node bifurcations, we can use local truncations. We will show that any face of $\mathcal{G}$ spanned by two primary edges and one secondary edge can be realized by a *suitable* 2-parameter family $K(d,\phi)$ of convex bodies (cf. Definition 10). Such a family has (among others) the property that it collapses to family described above if we restrict to any of the three edges of $\mathcal{G}$, so the existence of this suitable 2-parameter family proves the Theorem.

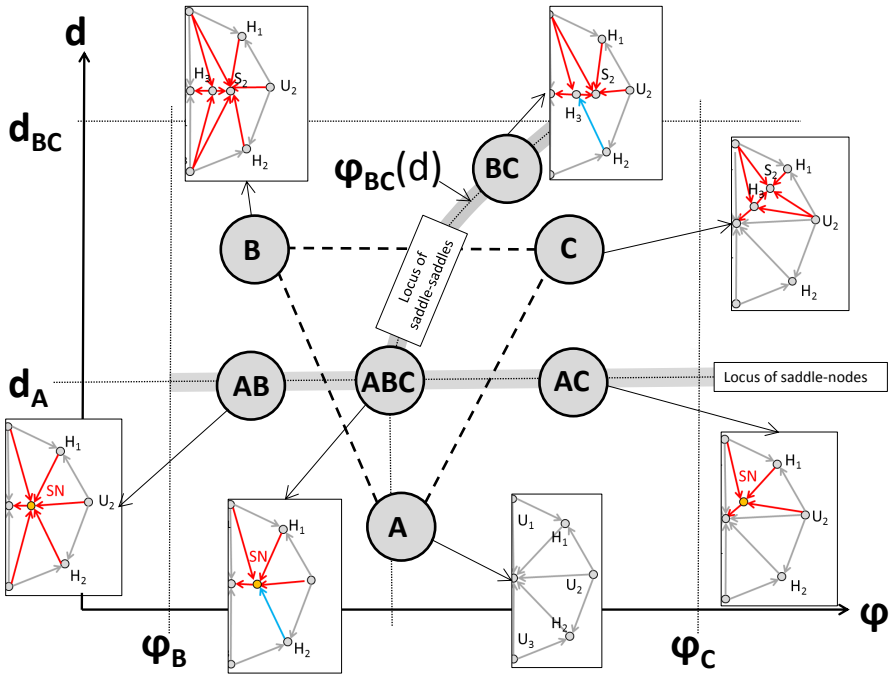

FIGURE 9. A codimension 2 bifurcation on a triangular face of the metagraph $\mathcal{G}$. The generic graphs A, B, C can be regarded as subgraphs of a topology graph. For example, by adding one stable point, they are identical to triangulated representations of the graphs (f,j,k) in figure 3. The degenerate graphs AB, AC, containing codimension 1 saddle-node bifurcations SN, correspond to primary edges fj, fk of $\mathcal{G}$. The degenerate graph BC, containing a codimension 1 saddle-saddle connection H2-H3 corresponds to the secondary edge jk of the metagraph. Finally, the degenerate graph ABC, containing the codimension 2 bifurcation, corresponds to the triangular face fjk of the metagraph $\mathcal{G}$

.

Let B and C be the primary graph representations of two gradient vector fields that are connected via any given saddle-saddle bifurcation. Furthermore, let A be their common ancestor, that is, B and C can be derived from A by twin vertex splittings. By Lemma 1, such a graph exists and from [8] we know that each of the three graphs A, B, C can be associated with the gradient vector fields of the smooth, convex bodies K_A, K_B, K_C, respectively. We denote the degenerate graphs belonging to the corresponding transitions by AB, AC, BC and ABC, respectively. See Figure 9.

Definition 10. A 2-parameter family $K(d, \phi)$ of convex bodies, where $d \in [0, d_{BC}]$ and $\phi \in [\phi_B, \phi_C]$ is called *suitable* if the function $(d, \phi) \mapsto K(d, \phi)$ is continuous with respect to Hausdorff distance, and there is a value $d_A \in (0, d_{BC})$ and a function $\phi_{BC} : [d_A, d_{BC}] \in (\phi_B, \phi_C)$ such that the following holds:

(10.1) for every $\phi \in [\phi_B, \phi_C]$, $K(0, \phi) = K_A$,
(10.2) for every $\phi \in [\phi_B, \phi_C]$ and $d < d_A$, the graph of $K(d, \phi)$ is homeomorphic to A,
(10.3) for every $d > d_A$ and $\phi < \phi_{BC}(d)$, the graph of $K(d, \phi)$ is homeomorphic to B,
(10.4) for every $d > d_A$ and $\phi > \phi_{BC}(d)$, the graph of $K(d, \phi)$ is homeomorphic to C,
(10.5) for every $\phi < \phi_{BC}(d_A)$, the graph of $K(d_A, \phi)$ is homeomorphic to AB,
(10.6) for every $\phi > \phi_{BC}(d_A)$, the graph of $K(d_A, \phi)$ is homeomorphic to AC,
(10.7) for every $d > d_A$, the graph of $K(d, \phi_{BC}(d))$ is homeomorphic to BC,
(10.8) the graph of $K(d_A, \phi_{BC}(d_A))$ is homeomorphic to ABC.

If the same properties hold *with the center of mass of K_A as a fixed reference point*, we say that $K(d, \phi)$ is *weakly suitable*.

This definition is illustrated in Figure 9. We remark that, in the context of Section 3, the line $\{d = d_A | \phi \in [\phi_B, \phi_C]\}$ and the curve $\{\phi = \phi_{BC}(d) | d \in [d_A, d_{BC}]\}$ form the bifurcation set associated with the gradient vector field.

We prove the assertion in two steps: in the first step (Subsection 4.1), we construct a weakly suitable family. In the second step (Subsection 4.2), we modify the construction in such a way that the center of mass of *every* member of the family coincides with that of K_A, showing that the previously constructed family is not only weakly suitable but can be made suitable.

4.1. **Neglecting the motion of the center of mass.** In the first step of the proof we assume that the graph of *every* convex body is taken with respect to the center of mass of K_A, i.e. we assume that the displacement of the center of mass does not influence the topology of the flow. For brevity we set $K = K_A$, and we consider only the case that the equilibrium point of K to be split is stable; if it is unstable, a similar argument with an arbitrarily small, conical extension of the surface can be applied.

Let s denote this stable point and the descendant points in the graphs B and C, obtained by splitting s, be s'_B, s''_B, s'_C, s''_C, respectively. Appealing to Lemma 5 of [8], we may assume that a neighborhood of s in ∂K belongs to a sphere $\mathbb{S}$. Without loss of generality, let the origin o be the center of this sphere, where the radius of $\mathbb{S}$ is assumed to be one. Furthermore, let c denote the center of mass of K, and note that, because s is a stable point, c is contained in the interior of the segment $[o, s]$.

Let Γ_i, where $i = 0, 1, 2, \ldots, m$ denote the edges of A starting at s, in counterclockwise order around s, from outside K. Clearly, for each value of i, the part of Γ_i in $\mathbb{S}$ is a great circle arc. These edges are labeled in such a way that the edges of B starting at s'_B correspond to the Γ_i's with $i = 1, 2, \ldots, k$ (and those starting at s''_B correspond to the remaining edges), and the edges starting at s'_C correspond to the Γ_is with $i = 1, 2, \ldots, k+1$ (and those starting at s''_C correspond to the remaining ones). Observe that, measured in counterclockwise order, either the angle from Γ_1 to Γ_{k+1}, or the angle from Γ_{k+1} to Γ_m is less than π. Without loss of generality, we may assume that the angle from Γ_1 to Γ_{k+1} is less than π.

First, we truncate the spherical neighborhood of s by a plane P sufficiently close to but outside s, and investigate the equilibrium points of the truncated body with

respect to c. In the generic case we have two possibilities for the graph of the truncated body K_P. If $K \cap P$ does not contain a new stable point, then the graph of K_P remains homeomorphic to A. Furthermore, if $K \cap P$ does contain a new stable point s'', then a new saddle point is created on $P \cap \partial K$, and every heteroclinic orbit on K intersecting P ends up at s (cf. Figure 10), whereas those not intersecting it remain the same. Finally, note also that $K \cap P$ contains a stable point if, and only if, the orthogonal projection of c onto P is contained in the interior of $K \cap P$. (If the projection is contained on the boundary of this circle, it is a degenerate case corresponding to a saddle-node bifurcation.) We will find a 2-parameter family of planes such that, if the intersection circle contains the projection of o on any member, then the edges meeting the circle are either $\Gamma_1, \ldots, \Gamma_k$, or $\Gamma_1, \ldots, \Gamma_{k+1}$: see Figure 10.

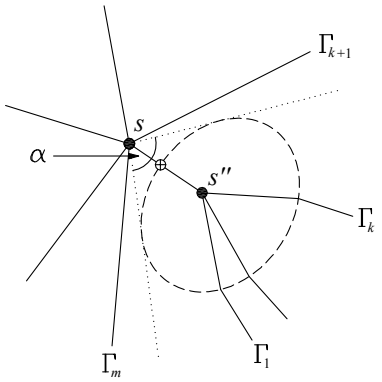

FIGURE 10. Truncation by the plane $P(d_{BC}, \theta, \phi)$ to create a body with graph B containing a new saddle on $P \cap \partial K$ and a sink s''.

An arbitrary plane in 3-space, and thus, in particular, the truncating plane, can be defined with three parameters. For this purpose we use the following coordinates:

(i) d: the depth of the cut (i.e. the height of the truncated spherical cap), measured from the point of the sphere where the tangent plane is parallel to the cutting plane;
(ii) θ: the arc distance of the center c_P of the intersection circle (the one created by the cutting plane on the sphere), from s, measured on $\mathbb{S}$;
(iii) ϕ: the angle of the great circle arc between c_P and s, and from some fixed great circle arc starting at s.

Up to a linear transformation, these parameters correspond to the polar coordinates of the vector pointing from the origin o to its orthogonal projection onto the truncating plane P, where the North Pole of $\mathbb{S}$ is s. Henceforth we denote the plane by $P(d, \theta, \phi)$.

Observe that, measured in counterclockwise order, we have $\angle(\Gamma_1, \Gamma_k) < \angle(\Gamma_1, \Gamma_{k+1}) < \angle(\Gamma_0, \Gamma_{k+1}) < \angle(\Gamma_0, \Gamma_{k+2})$. Choose some angle $0 < \alpha < \pi$ satisfying

$$\angle(\Gamma_1, \Gamma_{k+1}) < \alpha < \angle(\Gamma_0, \Gamma_{k+1}). \tag{11}$$

Furthermore, for any sufficiently small, fixed value $\theta > 0$, there is a value $d_{BC} = d_{BC}(\theta, \alpha)$ independent of ϕ such that for any plane P with parameters $P(d_{BC}, \theta, \phi)$,

α is the angle between the two great circle arcs on the sphere, starting at s and touching the intersection circle. Hence, by (11), there are some $\phi_B < \phi_{BC} < \phi_C$, with ϕ_B and ϕ_C depending only on α, and $\phi_{BC} = \phi_{BC}(d)$ depending on α and d, such that

(12)
- for any $\phi \in [\phi_B, \phi_{BC}(d))$ the plane $P(d_{BC}, \theta, \phi)$ intersects Γ_i if and only if $i = 1, 2, \dots, k$;
- the plane $P(d_{BC}, \theta, \phi_{BC}(d))$ intersects Γ_i if and only if $i = 1, 2, \dots, k$, and it is tangent to Γ_{k+1};
- for any $\phi \in (\phi_{BC}(d), \phi_C]$ the plane $P(d_{BC}, \theta, \phi)$ intersects Γ_i if and only if $i = 1, 2, \dots, k+1$ (cf. Figure 10).

Now, consider the one-parameter family $P(d_{BC}, \theta, \phi)$, with θ fixed and depending only on $\phi \in [\phi_B, \phi_C]$. If, for any value of ϕ in this interval, the projection of c lies on $K \cap P(d_{BC}, \theta, \phi)$, then, depending on the value of ϕ, the graph of the body truncated by the plane is homeomorphic to either B or C, or in the degenerate case to BC (cf. Figure 10). Since we intend to use local truncations only, we would like to guarantee this property for any sufficiently small value of $\theta > 0$. Before proceeding further, we recall two lemmas from [8].

Lemma 2. *Let $r > |s - c|$ and $\delta > 0$ be arbitrary. Then there is a convex body $K' \subseteq K$ satisfying the following:*

(i) *The graph of K' is homeomorphic to A.*
(ii) *Denoting the critical point of K' corresponding to s by s', s' has a spherical cap neighborhood in $\partial K'$, of radius arbitrarily close to r.*
(iii) *Denoting the integral curve of K' corresponding to Γ_i by Γ_i' for every i, and by t_i and t_i' the unit tangent vectors of Γ_i and Γ_i' at s', respectively, we have that $|t_i' - t_i| < \delta$.*

We note that the same statement is proven in [8] for the case that s is an unstable point, and the radius of its spherical neighborhood is arbitrarily close to any given value $0 < r < |s - c|$.

Lemma 3. *Let C be the unit circle in the plane $\mathbb{R}^2$ with the origin o as its center, and let $c = (0, \tau)$, where $\tau > 0$. Let $q_1 = (\mu_1, \nu_1)$ and $q_2 = (\mu_2, \nu_2)$ be two points of C such that $v_1 > 0$.*

(i) *If $[q_1, q_2]$ is perpendicular to $[s, q_1]$, then $\lim_{\mu_1 \to 0} \frac{\mu_2}{\mu_1} = \frac{2\tau}{1-\tau}$.*
(ii) *If the angle of $[q_1, q_2]$ and $[c, q_1]$ is $\frac{\pi}{2} - C\mu_1$ for some constant C' independent of μ_1, then $\lim_{\mu_1 \to 0} \frac{\mu_2}{\mu_1} = \frac{2\tau}{1-\tau} + 2C'$.*

Now, consider a plane $P = P(d_{BC}, \theta, \phi)$ with an arbitrary value of ϕ (cf. Figure 10), and let the closest and the farthest points of the circle $\bar{C} = P \cap \partial K$ from the segment $[o, s]$ be denoted by q_2 and q_1, respectively. For convenience, we imagine, for the moment, the plane containing $q_1 = (\mu_1, \nu_1)$, $q_2 = (\mu_2, \nu_2)$ and $c = (0, \tau)$ as $\mathbb{R}^2$ in Lemma 3: Figure 11.

For any sufficiently small $\theta > 0$, we require that the orthogonal projection of c on P lie in the interior of the segment $[q_1, q_2]$. Since $\angle(q_1, q_2, c) < \frac{\pi}{2}$, this property holds if and only if $\angle(q_2, q_1, c) < \frac{\pi}{2}$ for any sufficiently small $\theta > 0$. Recall that d_{BC} is defined by the fact that the angle of the two tangent lines of $\bar{C}$, passing

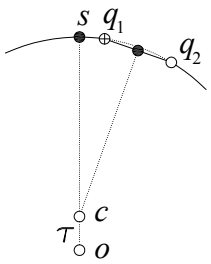

FIGURE 11. An illustration for Lemma 3. The sinks s and s'' (filled circles) and the saddle (circle with cross) of Figure 10 are identified.

through p, is equal to α. Let $\bar{C}^s$, q_1^s and q_2^s denote the central projections of $\bar{C}$, q_1 and q_2, respectively, onto the tangent plane of K at s. Then, as $\theta \to 0$, the limit of the angle of the two tangent lines of $\bar{C}_s$, passing through s, is equal to α. Thus, an elementary computation yields that, as $\theta \to 0$, the limit of the ratio of the x-coordinate of q_2^s to that of q_1^s is equal to $\frac{1+\sin\frac{\alpha}{2}}{1-\sin\frac{\alpha}{2}}$, implying that the same holds for $\lim_{\theta\to 0}\frac{\mu_2}{\mu_1}$.

We conclude that our requirement that the orthogonal projection of c on P lies inside $[q_1, q_2]$ for any sufficiently small $\theta > 0$ is satisfied if $\frac{2\tau}{1-\tau} < \frac{1+\sin(\alpha/2)}{1-\sin(\alpha/2)}$, but not if $\frac{2\tau}{1-\tau} > \frac{1+\sin(\alpha/2)}{1-\sin(\alpha/2)}$. To guarantee the former, we apply Lemma 3, and choose $\delta > 0$ sufficiently small, i.e., such that for the truncated body K' and heteroclinic orbits Γ_i, the inequalities (11) remain true with the same value of α. Let c' be the center of mass of K' and o' be the center of the spherical neighborhood of s. Furthermore, let $\tau' = \frac{|s-c'|}{|s-o'|}$. Note that for a suitable choice of r, we have $\frac{2\tau'}{1-\tau'} > \frac{1+\sin(\alpha/2)}{1-\sin(\alpha/2)}$.

According to the previous paragraph, with a little abuse of notation, we assume that for the *original body* K, for any sufficiently small $\theta > 0$, the orthogonal projection of c on $P = P(d_{BC}, \theta, \phi)$ lies in the interior of $P \cap K$. Let $d_A = d_A(\theta, \alpha)$ denote the value of d, independent of ϕ, at which the projection of c lies on the boundary of $P \cap K$.

We have shown that, for $\phi \in [\phi_B, \phi_C]$ and θ is sufficiently small, the intersection circle $P(d_{BC}, \theta, \phi) \cap K$ contains in its interior a new stable point with respect to c. Thus, the graph of any such truncated body $\bar{K}$ is homeomorphic to either B or C, or to BC. Then we fix a sufficiently small value of θ, and take the 2-parameter family of convex bodies $K(d, \phi)$, where $d \in [0, d_{BC}]$, and $\phi \in [\phi_B, \phi_C]$, defined as the truncation of K by the plane $P(d, \theta, \phi)$: see Figure 12). Finally, for any value of ϕ, $K(0, \phi) = K$, which shows that (10.1) in Definition 10 is satisfied. The remaining properties in Definition 10 of a weakly suitable family follow from (3). This completes the first step of the proof.

We note that the bifurcation diagram of Figure 9 in the geometric parameters d, ϕ used for the construction of the truncating plane and that of Figure 8(a) in the unfolding parameters μ_1, μ_2 of Section 3 are topologically *but not differentiably* equivalent. As noted in Section 3, the bifurcation curves meet in a tangency in Figure 8(a); however, they meet at a nonzero angle in Figure 9.

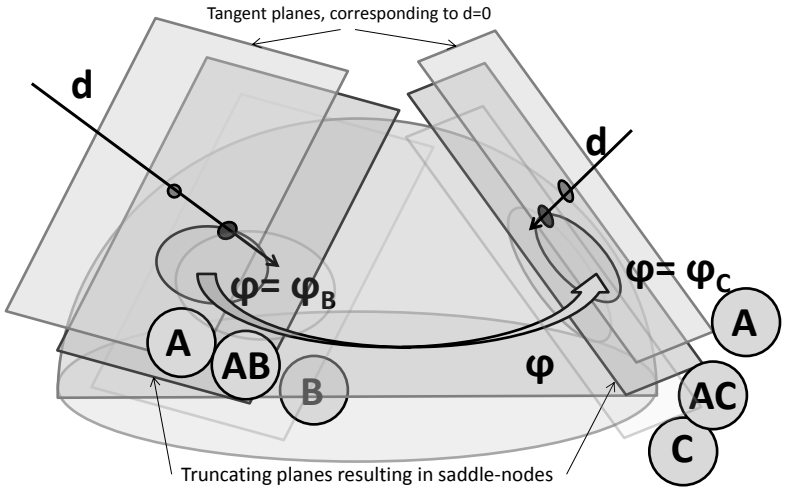

FIGURE 12. The 2-parameter family of truncations used in the construction. Variation of the angle ϕ of rotation of the truncating plane results either in a saddle-saddle bifurcation, or in no bifurcation. Variation of the depth d of the truncation results in a saddle-node bifurcation; the graphs belonging to the two extremal values of ϕ are identified with capital letters.

4.2. **Annihilating the motion of center of mass by an auxilary truncation.** In this subsection we modify the family $K(d, \phi)$ in such a way that the center of mass of every member in the modified family remains at c. To do this we need some additional assumptions on K.

Let L be the line passing through s and c, and let w denote the point of $L \cap \partial K$ different from s. We show that $K = K_A$ can be chosen in such a way that q is not an equilibrium point, and that it does not belong to any edge of A. First we modify the convex body K_0 in class $(1, 1)$ in [28] to satisfy this property. Since the graph of K_0 does not contain edges, we need only show that no line through the center of mass passes through more than one equilibrium point.

Since K_0 has D_4 rotational symmetry, in a suitable coordinate system, its two equilibrium points and center of mass c lie on the z-axis, and K_0 is symmetric with respect to the (x, y)-coordinate plane. Thus, all the tangent planes of K_0, parallel to the x-axis (i.e. satisfying the property that one of their translates contains the x-axis), touch K_0 at points in the (y, z)-plane. Clearly, cutting off a sufficiently small part of K_0 near the positive half of the x-axis does not change the number of equilibria nor the primary equilibrium class $\{1, 1\}$ of the body. The center of mass c' of the modified body K_0' is in the open half space $\{x < 0\}$. Hence, if the tangent plane of K_0' at some point p is perpendicular to the segment $[c', p]$, then the outer normal vectors of this plane have positive x-coordinates, implying that p is in the open half space $\{x > 0\}$. To show that any graph A can be associated to a convex body K_A satisfying this property, we observe that, by [8, Theorem 1], K_A can be obtained from K_0' by a finite sequence of local deformations.

In [8] we also showed that a neighborhood of any point of a non-isolated heteroclinic orbit, or a sink, or a source can be truncated by a sphere without changing the class of the graph of the body. Furthermore, by [8, Lemma 1], we obtain that, applying a sufficiently small truncation at w, the line connecting the modified stable point and the modified center of mass intersects this spherical surface. Thus, we may also assume that a neighborhood of w is a sphere $\mathbb{S}'$. Nevertheless, note that the center of $\mathbb{S}'$ is not necessarily on the line L. Let $c_{d,\phi}$ denote the center of mass of the *truncated* spherical cap $G(d,\phi)$ near s. To obtain a modified body $K'(d,\phi)$, we truncate K_A near q by a second plane $P'(d',\theta',\phi')$, such that the center of mass of the union of B, and the second truncated (open) spherical cap G', is c (cf. Figure 13). Clearly, in this case the center of mass of the doubly truncated body $K'(d,\phi)$ is identical to the center of mass c of K.

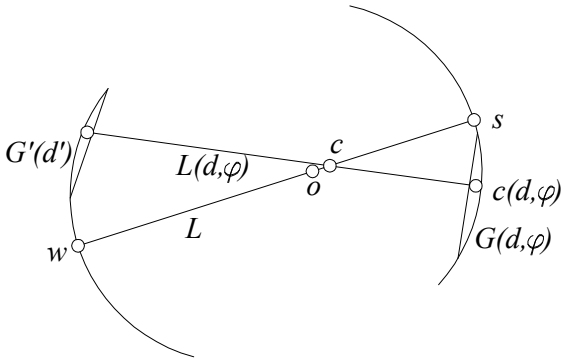

FIGURE 13. The second truncation near the critical point w opposite to s; the circular arcs lie on the spherical caps G and G'.

Let $L(d,\phi)$ denote the line connecting c and $c(d,\phi)$. First, let d' be fixed. Then, changing θ' and ϕ', the locus of the centers of mass of G' is a part of a sphere $\mathbb{S}'_{d'}$, concentric to $\mathbb{S}'$, and the radius of this sphere depends on d' and $\mathbb{S}'$ only. Thus, if $\theta > 0$ is sufficiently small, for every line $L(d,\phi)$ and every (small) value of d' there is a unique position of G' such that its center of mass lies on $L(d,\phi)$. Let us call this cap $G' = G'(d')$. Note that the center of mass of the union of $G(d,\phi)$ and $G'(d')$ is c if and only if, the torques about c exerted by the two caps are equal. Here, the distance of the center of mass of $G'(d')$ from c is approximately $|q-c|$; that is a fixed value. Thus, by continuity, for every pair of values d,ϕ, there is at least one value of d' such that the center of mass of $G(d,\phi) \cup G'(d')$ is c. Let $G'(d,\phi)$ be the spherical cap $G'(d')$, where d' is the smallest value for which this property holds. Then, clearly, $G'(d,\phi)$ depends continuously on d and ϕ, and the 2-parameter family $K \setminus (G(d,\phi) \cup G'(d,\phi))$ has the required properties.

5. Summary

In this paper we showed that the secondary classification of smooth convex solids, based on the Morse-Smale complexes of their gradient vector fields, is not only complete in the sense that all combinatorially possible Morse-Smale complexes can

be realized on smooth, convex bodies, but it is also complete in the more general, 'dynamical' sense that all generic transitions between Morse-Smale complexes represented by non-isomorphic abstract graphs can be realized on one-parameter families of convex bodies. Among trajectories of physical convex shape evolution processes we find examples of such transitions, so our result implies that from a purely geometrical viewpoint, there is no restriction on these trajectories.

Theorem 3 admits only one-parameter families exhibiting one single bifurcation. However, if we only admit saddle-node bifurcations then, based on our argument in Section 4 we can formulate a more general claim. A codimension one, generic saddle-node is either a *creation* or an *annihilation*, depending on whether the number of generic critical points increases or decreases by two. As stated before, at saddle-saddle bifurcations the number of generic critical points does not change.

To formulate the claim we introduce

Definition 11. A generic, one-parameter family $v(\lambda)$ of gradient vector fields on the 2-sphere is called strictly monotone if it contains either only creations or only annihilations and it does not contain any saddle-saddle bifurcations.

Using this concept, we can state the following corollary to Theorem 3:

Corollary 1. For any generic, strictly monotone, one-parameter family $v(\lambda)$ of gradient vector fields on the 2-sphere there exists a one-parameter family $K(\lambda)$ of (not necessarily smooth) convex bodies such that $\nabla r_{K(\lambda)}$ is topologically equivalent to $v(\lambda)$ for every value of λ.

To extend this statement further, we make

Conjecture 1. Every equivalence class on the family of convex bodies, defined by the tertiary classification system, is connected. That is, for any two convex bodies K_1 and K_2 with the same topology graph A there is a one-parameter family $K(\lambda)$ of convex bodies, where $\lambda \in [0, 1]$, such that $K(0) = K_1$, $K(1) = K_2$, and the graph of $K(\lambda)$ is A for every value of λ.

If Conjecture 1 is true, Corollary 1 can be extended to include not only strictly monotone, but also generic families. Although our techniques do not admit the investigation of tertiary edges of $\mathcal{G}$, we also formulate

Conjecture 2. All tertiary edges of $\mathcal{G}$ are physical.

Regarding geophysical applications, we remark that in primary class $\{2, 2\}$ one of the secondary classes (that of ellipsoids) appears to be dominant and the other appears to be entirely missing among natural pebble shapes. Our results show that one *could* continuously transform members of one class into members of the other class. Apparently, this process exists in natural abrasion only in one direction.

6. Acknowledgments

This work was supported by OTKA grant T104601 and the János Bolyai Research Scholarship of the Hungarian Academy of Sciences. Comments from Timea Szabó are gratefully acknowledged.

References

[1] D. Archdeacon, J. Hutchinson, A. Nakamoto, S.Negami, and K. Ota. Chromatic numbers of quadrangulations on closed surfaces. *J. Graph Theory*, 37:100–114, 2001.

[2] V. Arnold. *Ordinary Differential Equations*. MIT Press, Cambridge, 1998.

[3] F. J. Bloore. The shape of pebbles. *Math. Geology*, 9:113–122, 1977.

[4] G. Brinkmann, S. Greenberg, C. Greenhill, B. McKay, R. Thomas, and P. Wollan. Generation of simple quadrangulations of the sphere. *Discrete Math.*, 305:22–54, 2005.

[5] G. Domokos. Monotonicity of spatial critical points evolving under curvature driven flows. *Journal of Nonlinear Science*, 25, 2015.

[6] G. Domokos, D. Jerolmack, A. A. Sipos, and A. Török. How river rocks round: Resolving the shape-size paradox. *PloS One*, 9:e88657, 2014.

[7] G. Domokos and Z. Lángi. The robustness of equilibria on convex solids. *Mathematika*, 60:237– 256, 2014.

[8] G. Domokos, Z. Lángi, and T. Szabó. The geneaology of convex solids. *arxiv preprint*, http://arxiv.org/abs/1204.5494, 2013.

[9] G. Domokos, T. Szabó, P. Várkonyi, and A. Sipos. Pebbles, shapes and equilibria. *Mathematical Geosciences*, 42:29–47, 2010.

[10] S. Dong, P. Bremer, M. Garland, V. Pasucci, and J. Hart. Spectral surface quadrangulation. *ACM T. Graphic*, 25:1057–1066, 2006.

[11] H. Edelsbrunner, J. Harer, and A. Zomorodian. Hierarchical Morse-Smale complexes for piecewise linear 2-manifolds. *Discrete Comput. Geometry*, 30:87–107, 2003.

[12] W. Firey. The shape of worn stones. *Mathematika*, 21:1–11, 1974.

[13] J. Gross and J. Yellen. *Graph Theory and Its Applications*. CRC Press, Boca Raton, FL, 2006.

[14] J. Guckenheimer and P. Holmes. *Nonlinear Oscillations, Dynamical Systems and Bifurcations of Vector Fields*. Springer, New York, 1983. Sixth Edition, 2002.

[15] D. Hilbert and S. Cohn-Vossen, editors. *Geometry and the Imagination*. AMS Chelsea Publishing, 1952.

[16] P. Holmes and D. Rand. Bifurcations of the forced van der Pol oscillator. *Quart. Appl. Math.*, 35:495–509, 1978.

[17] I. J. Pebble shape (and size!). *J. Sedimentary Research*, 61:756–767, 1991.

[18] D. Jerolmack. Pebbles on Mars. *Science*, 340:1055–1056, 2013.

[19] K. Miller, T. Szabó, D. Jerolmack, and G. Domokos. Quantifying the significance of abrasion and selective transport for downstream fluvial grain size evolution. *Journal of Geophyiscal Research / Earth Surface*, 119:24122429, 2014.

[20] J. Milnor, editor. *Morse Theory*. Princeton University Press, 1963.

[21] A. Nakamoto. Generating quadrangulations of surfaces with minimum degree at least 3. *J. Graph Theory*, 30:223–234, 1999.

[22] S. Negami and A. Nakamoto. Diagonal transformations of graphs on closed surfaces. *Sci. Rep. Yokohama Nat. Univ., Sec. I*, 40:71–97, 1993.

[23] L. Rayleigh. The ultimate shape of pebbles, natural and artificial. *Proc. R. Soc. London A*, 181:107–118, 1942.

[24] L. Rayleigh. Pebbles, natural and artificial. Their shape under various conditions of abrasion. *Proc. R. Soc. London A*, 182:321–334, 1944.

[25] L. Rayleigh. Pebbles of regular shape and their production in experiment. *Nature*, 154:161–171, 1944.

[26] J. Sotomayor. Generic one-parameter families of vector fields on two-dimensional manifolds. *Bull. Amer. Math. Soc.*, 74:722–726, 1968.

[27] Z. T. Beitrag zur schotteranalyse. *Schweiz Mineral Petrogr Mitt.*, 15:39–140, 1935.

[28] P. Várkonyi and G. Domokos. Static equilibria of rigid bodies: dice, pebbles and the Poincaré-Hopf theorem. *Journal of Nonlinear Science*, 16:255–281, 2006.

[29] R. Williams, J. Grotzinger, W. Dietrich, S. Gupta, and D. Sumner. Martian fluvial conglomerates at Gale crater. *Science*, 340:1068–1072, 2013.

[30] A. Zomorodian, editor. *Topology for computing*. Cambridge University Press, 2005.

Gábor Domokos, Dept. of Mechanics, Materials and Structures, Budapest University of Technology, Műegyetem rakpart 1-3., Budapest, Hungary, 1111

E-mail address: domokos@iit.bme.hu

Zsolt Lángi, Dept. of Geometry, Budapest University of Technology, Egry József u. 1., Budapest, Hungary, 1111

E-mail address: zlangi@math.bme.hu

Philip Holmes, Program in Applied and Computational Mathematics and Dept. of Mechanical and Aerospace Engineering, Princeton University, Princeton NJ 08544

E-mail address: pholmes@math.princeton.edu